Chapter 4

DYNAMIC ANALYSIS

This chapter discusses the dynamic analysis of inflatable dams. After obtaining the equilibrium configurations, as explained in Chapter 3, small vibrations are considered about this configuration. Vibrations of the dam without water, with water, and with parallel flow are considered. Vibration frequencies are computed and the corresponding mode shapes are obtained.

4.1 LINEAR VIBRATIONS: FORMULATION

4.1.1 WITHOUT EXTERNAL WATER

The matrix equation of motion of an inflated dam for small motions about its equilibrium position has the form

$$M\ddot{U} + KU = 0 \tag{1}$$

where U represents the vector of global nodal displacements and M and K are the global mass and stiffness matrices, respectively, of the dam at its equilibrium position. All the matrices in equation (1) are real and symmetric. Standard procedures are used by ABAQUS to obtain the eigenvalues and eigenvectors for simple harmonic motion, and hence the vibration frequencies and modes.

4.1.2 WITH EXTERNAL WATER

In this case, the matrix equation of the dam for small motions about its equilibrium position takes the form

$$M\ddot{U} + KU = R \tag{2}$$

where R is the global force vector acting on the dam due to *p*, which is the change in total pressure of the water due to small motions of the dam about its equilibrium position and due to the external flow of water, with velocity U_p, parallel to the dam. The fluid flow is assumed to be inviscid and irrotational and the fluid is assumed to be incompressible so that the fluid velocities are given by $\vec{V} = \nabla\phi$ where ϕ is a velocity potential. Equation (2) defines a typical fluid-structure interaction problem. Several approaches have been proposed to solve such problems. In the present study, we use the "dry" mode shape functions $\psi_j(\vec{x})$ **(**mode shapes obtained after considering the hydrostatic pressure effects but not the dynamic effects (i.e., added mass)) as basis vectors to define the "wet" modes. Here, $\vec{x}$ = (*x*, *y*, *z*). Let $\psi_j(\vec{x})$ have Cartesian components (u_j, v_j, w_j). Then the displacement of an arbitrary point on the surface of the dam, due to the corresponding mode, can be written as $\xi_j(t)\psi_j(\vec{x})$ where $\xi_j(t)$ is the time-dependent amplitude for mode j. The body surface region S_b is defined as that part of the structure in contact with the external hydrostatic water (Figure 4.1). The normal component of $\psi_j(x)$ on S_b is expressed in the form (Newman, 1994)

$$n_j = \psi_j \,.\, \vec{n} = u_j n_x + v_j n_y + w_j n_z \tag{3}$$

The unit normal vector $\vec{n}$ points out of the fluid domain and into the body. Corresponding to these modes of motion, the generalized pressure forces (Figure 4.2) are defined in the form (Newman, 1994)

$$R_j = \iint_{S_b} p\, n_j \, dS \tag{4}$$

In the present analysis, wave and structural damping effects are neglected, and only the added mass effect is considered. In order to determine the added mass, we need to determine the fluid motion associated with the vibration of the structure. An *xyz* coordinate frame is used with the *z* axis pointing vertically upwards and the *xy* plane coinciding with the undisturbed free surface. We denote the wetted surface of the structure by S_b and the fluid domain by D. We assume that the fluid is bounded by S_b, the bottom S_h, the free surface S_f, two side surfaces S_s, and a surface S_∞ far away from the structure (Figure 4.1). The distance from S_∞ to the structure is taken to be approximately 40 m. It was found that for this distance the boundary condition on S_∞ does not influence the numerical results.

Assuming time-harmonic motion at frequency ω, the amplitude $\xi_j(t)$ for each mode can be written as the real part of $\hat{\xi}_j\, e^{i\omega t}$. The total velocity potential can be written as

$$\phi = \sum_j \xi_j(t)\ \phi_j(\vec{x}) \tag{5}$$

In the fluid domain, each velocity potential satisfies the Laplace equation

$$\nabla^2 \phi_j = 0 \tag{6}$$

Assuming that the frequency of oscillation is high, the free-surface boundary condition reduces to the infinite-frequency limit of

$$\phi_j = 0 \tag{7}$$

In this case, no waves are generated by the free surface. The velocity potentials on S_b must satisfy the boundary condition that the velocity of the fluid on the dam is the equal to that of the dam

$$\frac{\partial \phi_j}{\partial n} = (V_n)_j = U_p \frac{\partial n_j}{\partial y} + i\omega n_j \tag{8}$$

and those on the bottom surface S_h, the two side surfaces S_s, and the surface $S_{\circlearrowleft}$ must satisfy the no penetration condition

$$\frac{\partial \phi_j}{\partial n} = (V_n)_j = 0 \tag{9}$$

The velocity potentials are found using a boundary integral method. Following Hess and Smith (1964), who were the first to develop the method to a practical stage, Green's theorem with an appropriate Green's function is used to reduce the problem to solving an integral equation on the fluid boundary. We define a Green's function G consisting of a Rankine source and its image above the free surface. We write

$$G(\vec{x}, \vec{\chi}) = \frac{1}{r} - \frac{1}{r'} \tag{10}$$

where

$\vec{x} = (x, y, z)$ is the field point

$\vec{\chi} = (\chi, \eta, \zeta)$ is the source point

$r^2 = (x - \chi)^2 + (y - \eta)^2 + (z - \zeta)^2$

$(r')^2 = (x - \chi)^2 + (y - \eta)^2 + (z + \zeta)^2$

Application of Green's second identity provides a Fredholm equation of the second kind for the values of the potential on the boundaries:

$$\phi_j(\vec{x}) + \iint_{\partial D} \phi_j(\vec{\chi}) \frac{\partial G(\vec{x}, \vec{\chi})}{\partial n_{\vec{\chi}}} dS_{\vec{\chi}} = \iint_{\partial D} V_{n_j}(\vec{\chi})\ G(\vec{x}, \vec{\chi})\, dS_{\vec{\chi}} \tag{11}$$

The fluid boundary ∂D consists of the body boundary S_b, the bottom S_h, two side surfaces S_s, and the surface $S_{\circledcirc}$. The free surface S_f is not discretized since the Green's function G satisfies the free-surface condition.

The integral equation (11) is solved numerically by replacing the body surface region S_b, the bottom S_h, and the surface $S_{\circledcirc}$ by an ensemble of quadrilateral elements of constant potential strength. In this study, 300 panels were used on S_b, 55 on each S_s, and 60 on $S_{\circledcirc}$. The results were found to be unaffected by the number of panels if more were used. Then the integral equation is satisfied at a set of collocation points (in this study the panel centroids are used), resulting in a linear system of equations for the unknown potential values. From the values of the velocity potentials on the body surface, the pressure on the dam and hence the added mass values may be obtained by using the standard definitions :

$$p_j = -[i\rho\omega\phi_j - \rho U_p \frac{\partial \phi_j}{\partial y}]e^{i\omega t} \tag{12}$$

Substituting the expression for pressure p_j in equation (4), we get

$$R_i = \rho e^{i\omega t} \iint_{S_b} [-i\omega\phi_j - U_p \frac{\partial \phi_j}{\partial y}] n_i \, dS \tag{13}$$

But R_i can be expressed as

$$R_i = -M_{ij}\ddot{\xi}_j - B_{ij}\dot{\xi}_j \tag{14}$$

Replacing $\xi_j(t)$ by $\hat{\xi}_j e^{i\omega t}$, we get

$$R_i = [\omega^2 M_{ij} - i\omega B_{ij}]\hat{\xi}_j e^{i\omega t} \tag{15}$$

By comparing equations (13) and (15), we get

$$(M_A)_{ij} - \frac{i}{\omega} B_{ij} = -\frac{i\rho}{\omega}\iint_{S_b} \phi_j n_i \, dS - \frac{\rho U_p}{\omega^2}\iint_{S_b} \frac{\partial \phi_j}{\partial y} n_i dS \tag{16}$$

The change in pressure acts as additional inertia on the structure. Thus equation (2) now becomes

$$(M_g + M_A)\ddot{\xi} + B\dot{\xi} + K_g\,\xi = 0 \tag{17}$$

where M_g and K_g are the generalized mass and stiffness matrices, respectively, of the dam at its equilibrium position, M_A is the added mass matrix of the structure, and B is the damping matrix of the structure. The matrices M_g and K_g are of dimension equal to the number of modes and obtained from ABAQUS. All the matrices in equation (17) are real and symmetric. In the present study the values of the damping coefficients were found to be small compared to the other values in equation (17). This should be expected since in the infinite-frequency limit, no waves are generated on the free surface and hence there is no wave damping. Replacing $\xi(t)$ by $\hat{\xi}\,e^{i\omega t}$ and neglecting damping, we can rewrite equation (17) as

$$[-\omega^2 (M_g + M_A) + K_g]\hat{\xi} = 0 \tag{18}$$

Standard procedures can be utilized to solve the above eigenvalue problem to obtain the new natural frequencies and the eigenvectors. The eigenvectors can then be used along with the "dry" mode shapes to obtain the "wet" mode shapes.

4.2 LINEAR VIBRATIONS: RESULTS

4.2.1 PROCEDURE VALIDATION

To validate the procedure adopted to compute the natural frequencies of the structure with or without external water, two example cases are chosen.

In the first example, a long circular cylindrical shell of length 80 m and radius 1 m is considered. The purpose of using this model is to use the known analytical results for frequencies, added mass, and mode

shapes to compare the results obtained by using the numerical procedures discussed in Section 4.1. First, the structure is assumed to vibrate in air. The structure is assumed to be pinned at the ends and is restrained so as to allow vibrations only in a plane. The structure is modeled as a shell using 128 quadrilateral shell elements of the type S4R in ABAQUS, and the first four natural modes and frequencies of vibration are obtained. The length is much larger than the radius so that the numerical results should be close to the analytical results for a pinned-pinned beam. As is well known, the natural frequencies and mode shapes of a pinned-pinned beam are given by

$$\omega_n = \frac{n^2 \pi^2}{L^2} \sqrt{EI / \mu} \tag{19}$$

$$y_n = \sin\left(\frac{n\pi x}{L}\right) \tag{20}$$

where L is the length, EI is the bending stiffness, and μ is the mass per unit length of the beam.

The frequencies and mode shapes obtained numerically are in close agreement with those obtained from equations (19) and (20). The cylinder is then assumed to be completely submerged in water far away from the free surface so that free surface effects are not important. Because the length of the structure is much greater than its diameter, strip theory can be used to obtain the added mass coefficients for the first four mode shapes analytically. The vibration frequencies of the structure completely submerged in water are obtained by using Rayleigh's Quotient:

$$\omega_n^2 = \frac{\int_L EI \left(\frac{d^2 y_n}{d x^2} \right)^2 dx}{\int_L (\mu + m_A)\, y_n^{\,2}\, dx} \tag{21}$$

where y_n is the mode shape and $m_A = \rho \Pi R^2$, the sectional added mass of a 2-D cylinder. Here, ρ is the density of the water. These frequencies are obtained one at a time for each mode of vibration by using mode shapes y_n given by equation (20).

Numerical values for the added mass coefficients and the natural frequencies are then obtained using the procedure discussed in Section 3. A total of 256 panels (128 on the cylindrical surface and 64 each on the two ends of the cylinder) are used to discretize the body surface. The added mass values obtained numerically are in close agreement with those obtained by using strip theory and the numerical values of the natural frequencies closely match those obtained from equation (21). Table 4.1 shows the natural frequencies of the cylinder without and with water.

In the second example, the procedure is applied to compute the first four vibration modes and frequencies of the double-anchored inflatable dam (Figure 4.3) which was considered by Dashina Moorthy et al. (1995). The vibration frequencies and mode shapes of the dam both in the presence and absence of external water are computed. The vibration frequencies (Table 4.2) and mode shapes obtained are in close agreement with those obtained by Dakshina Moorthy et al. (1995). The maximum difference in the first four frequencies is 10 percent without water and 11 percent with water. The difference in frequencies can be attributed to the size of the mesh considered (500 elements in present case and 200 in the example considered), and the type of shell element chosen (four-noded element in present case and nine-node element in the example considered). The frequencies were found to reduce in presence of external water as was found by Dakshina Moorthy (1995).

4.2.2 NUMERICAL RESULTS

4.2.2.1 WITHOUT EXTERNAL WATER

Consider dams that are not impounding water. For the vibration analysis the dam is clamped at the ends once the equilibrium shape is obtained. Small three-dimensional vibrations are then considered about the equilibrium configuration.

The first four vibration frequencies and mode shapes are computed. The results are presented in Figures 4.4-4.8. Figure 4.4 shows the variation of the frequencies with internal pressure for the first four vibration modes, and Table 4.3 lists the corresponding frequencies for p_{int} = 1 kPa and 30 kPa. The slopes of the curves in Figure 4.4 decrease as the internal pressure increases. The vibration frequencies increase with the internal pressure, as one would expect. The squares of the frequencies vary almost linearly with the internal pressure. Figures 4.5 and 4.7 depict the first four vibration mode shapes for internal pressures of 1 kPa and 30 kPa, respectively. The first and second modes are symmetric and the third and fourth modes are anti-symmetric longitudinally. The corresponding profiles of the central cross-section for these modes (solid curves) and the cross-sections at a distance of one-quarter length from each end (dashed curves) are illustrated in Figures 4.6 and 4.8 for internal pressures of 1 kPa and 30 kPa, respectively. For the modes that are symmetric longitudinally, the two dashed curves are identical.

4.2.2.2 WITH EXTERNAL WATER

For the case of the dam impounding water on one side, the dam is clamped along the equilibrium cross-sections at its two ends, and then water is applied on the anchored side with a height less than the "dry" equilibrium height. The new equilibrium configuration is obtained and small vibrations of the dam about this equilibrium shape are analyzed. The results are presented in Figures 4.9-4.13. Figure 4.9 depicts the variation of the first four frequencies with the external water head, for an internal pressure p_{int} = 30 kPa. The frequencies tend to decrease first and then increase as the external water head increases. The frequencies for the higher modes (modes 3 and 4) show more variation compared to those for the lower modes (modes 1 and 2). The frequencies are high enough to justify the infinite-frequency limit

assumption used to define the boundary condition on the free-surface. Table 4.3 compares the vibration frequencies of the dam with no external water to those for the dam in the presence of external hydrostatic pressure (with no added mass effect), for p_{int} = 1 kPa and 30 kPa. The external water head is 0.5 m and 1.5 m, respectively.

The corresponding first four modes are depicted in Figures 4.10 and 4.12, respectively. The frequencies of the structure in the presence of water are lower than those in the absence of water by a maximum of 11.3 percent in Table 4.3. The first and second modes are symmetric and the third and fourth modes are anti-symmetric longitudinally. Figures 4.11 and 4.13 show the cross-sectional behavior of the modes at the half-length (solid curves) and quarter-lengths (dashed curves) from each end of the dam for internal pressures of 1 kPa and 30 kPa, respectively. In Figures 4.11 and 4.13, the horizontal line at the left of the dam indicates the water height. For the first two modes the two dashed curves are identical. The cross-sectional behavior of the dam in the presence of external water, at half-length and quarter-lengths from the ends, is similar to that of the dam in the absence of water for both the internal pressures.

4.2.2.3 WITH PARALLEL FLOW

The case of the dam impounding water flowing parallel to the dam is considered. This situation may occur for a dam deployed along a river. In this case, the dam is clamped along the equilibrium cross-sections at its two ends, and then parallel flowing water is applied on the anchored side with the same height as that in the case of hydrostatic water (Section 4.2.2.2). The equilibrium configuration is the same as that obtained for the case of the dam impounding hydrostatic water. Small vibrations of the dam about this equilibrium shape are analyzed. The direction of the flow is from the nearer end to the farther end along the length of the dam in Figures 4.14-4.21. The flow introduces hydrodynamic pressure and thus the boundary conditions on the structure change due to the fluid-structure interaction.

The vibration analysis was performed for internal pressures of 1 kPa and 30 kPa, as in the earlier cases. Flow velocities of 1 m/s and 5 m/s were considered. The natural frequencies and the corresponding mode shapes were obtained using the procedures described in Section 4.1.2. Figures 4.14-4.21 illustrate the effect of parallel flow on the vibration behavior of the dam. The frequencies of vibration for the dam with internals pressure of 1 kPa and 30 kPa are presented in Tables 4.4 and 4.5, respectively. The frequencies reduce by a maximum of 16.4 percent and 17.2 percent in Tables 4.4 and 4.5, respectively.

For the dam with internal pressure of 1 kPa, Figures 4.14 and 4.16 depict the mode shapes for flow velocities of 1 m/s and 5 m/s. Figures 4.15 and 4.17 illustrate the corresponding cross-sectional shapes at the center and quarter lengths from the ends of the dam. Figures 4.18 and 4.20 depict the mode shapes of the dam with internal pressure of 30 kPa, for flow velocities of 1 m/s and 5 m/s. Figures 4.19 and 4.21 illustrate the corresponding cross-sectional shapes at the center and quarter-lengths from the ends of the dam. In all the above cases, the first and second modes are symmetric and the third and fourth modes are anti-symmetric longitudinally. Thus, the cross-sectional behavior of the dam in the presence of external parallel flow, at half-length and quarter-lengths from the ends, is similar to that of the dam in the absence of water for both the internal pressures.

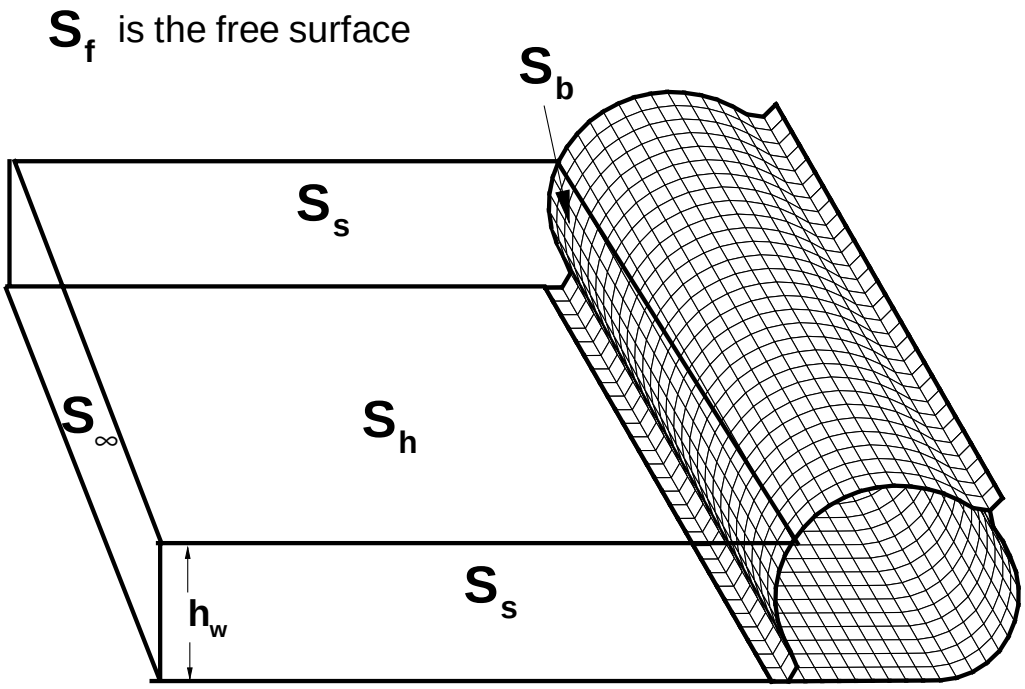

Schematic diagram representing the boundary value domain

Figure 4.1 Schematic diagram representing the boundary value domain.

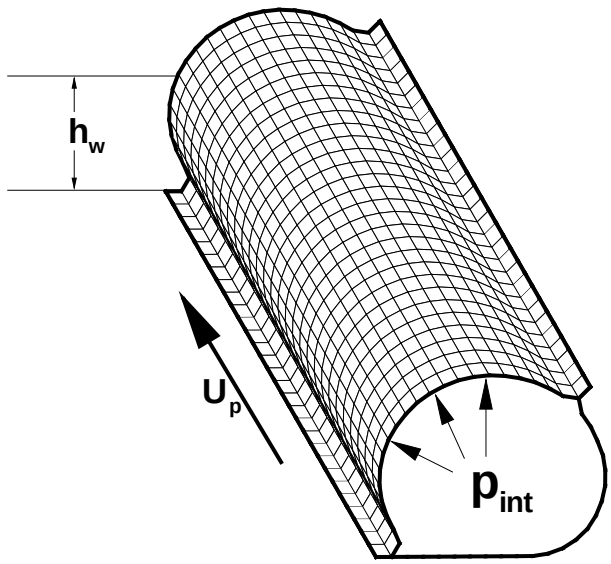

Schematic diagram showing the pressure forces on the dam

Figure 4.2 Schematic diagram showing the pressure forces on the dam.

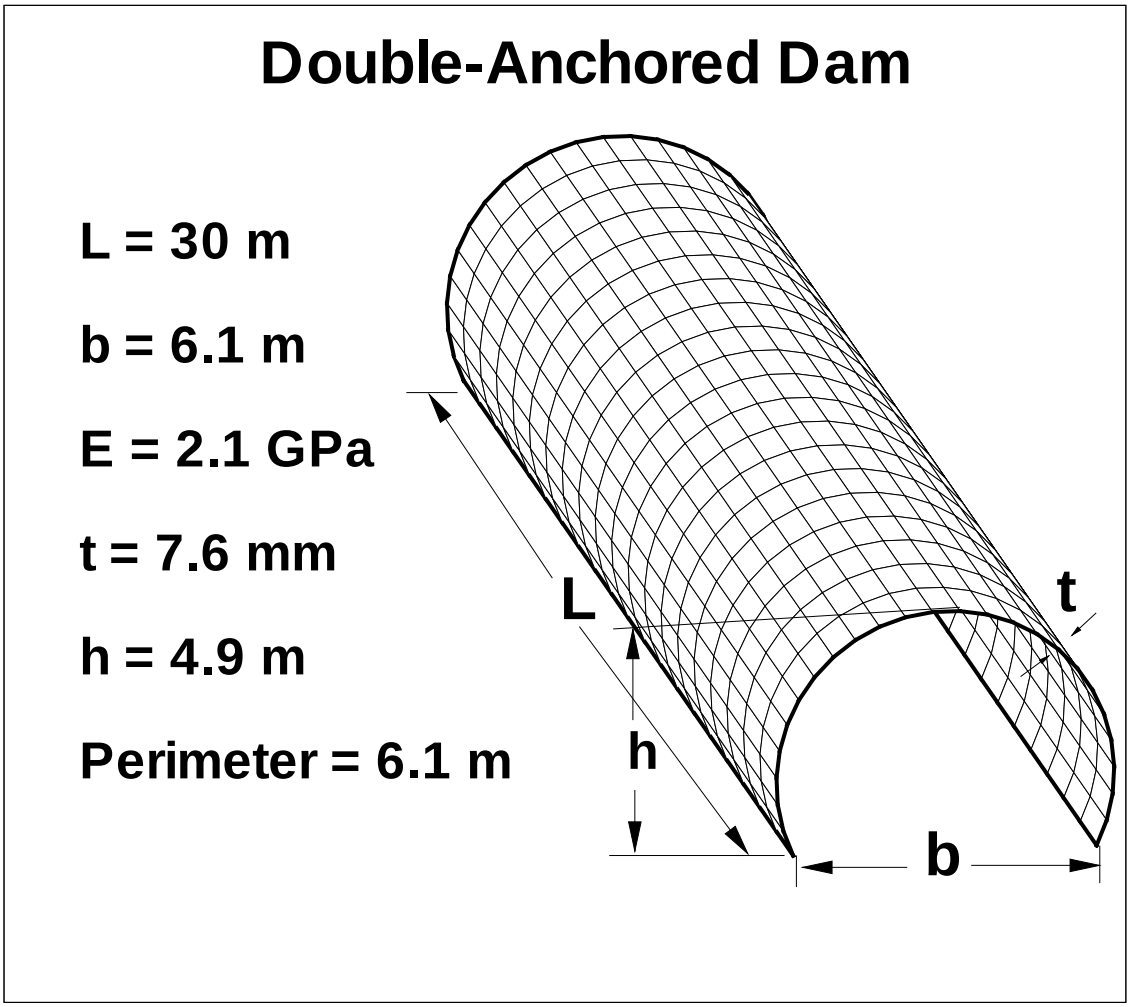

Figure 4.3 Model information for the double-anchored dam used by Dakshina Moorthy et al. (1995).

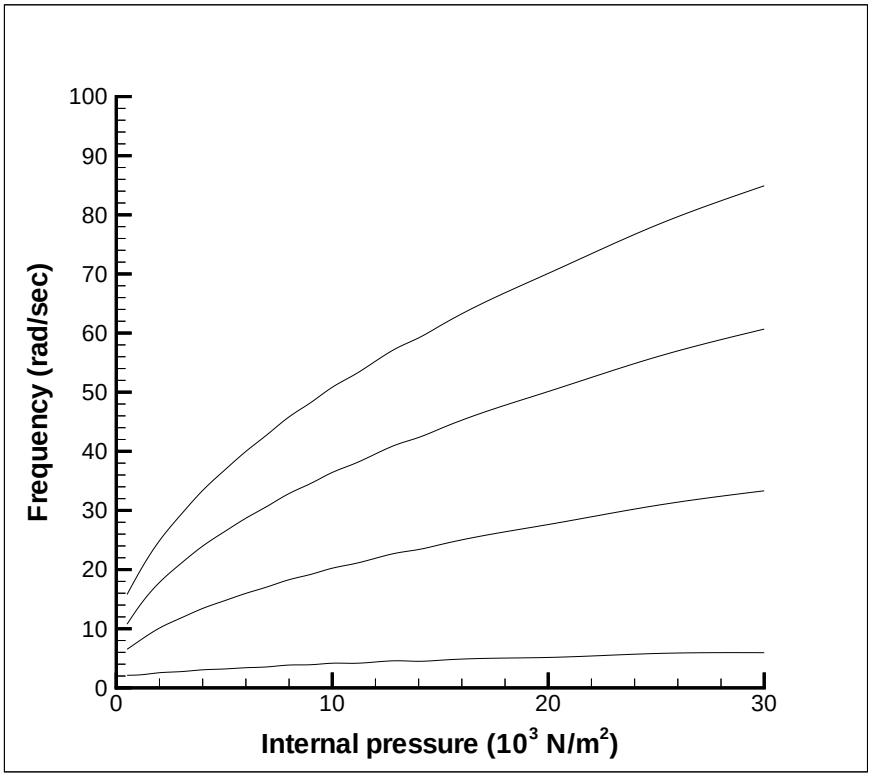

Figure 4.4 Variation of frequencies with internal pressure, without water.

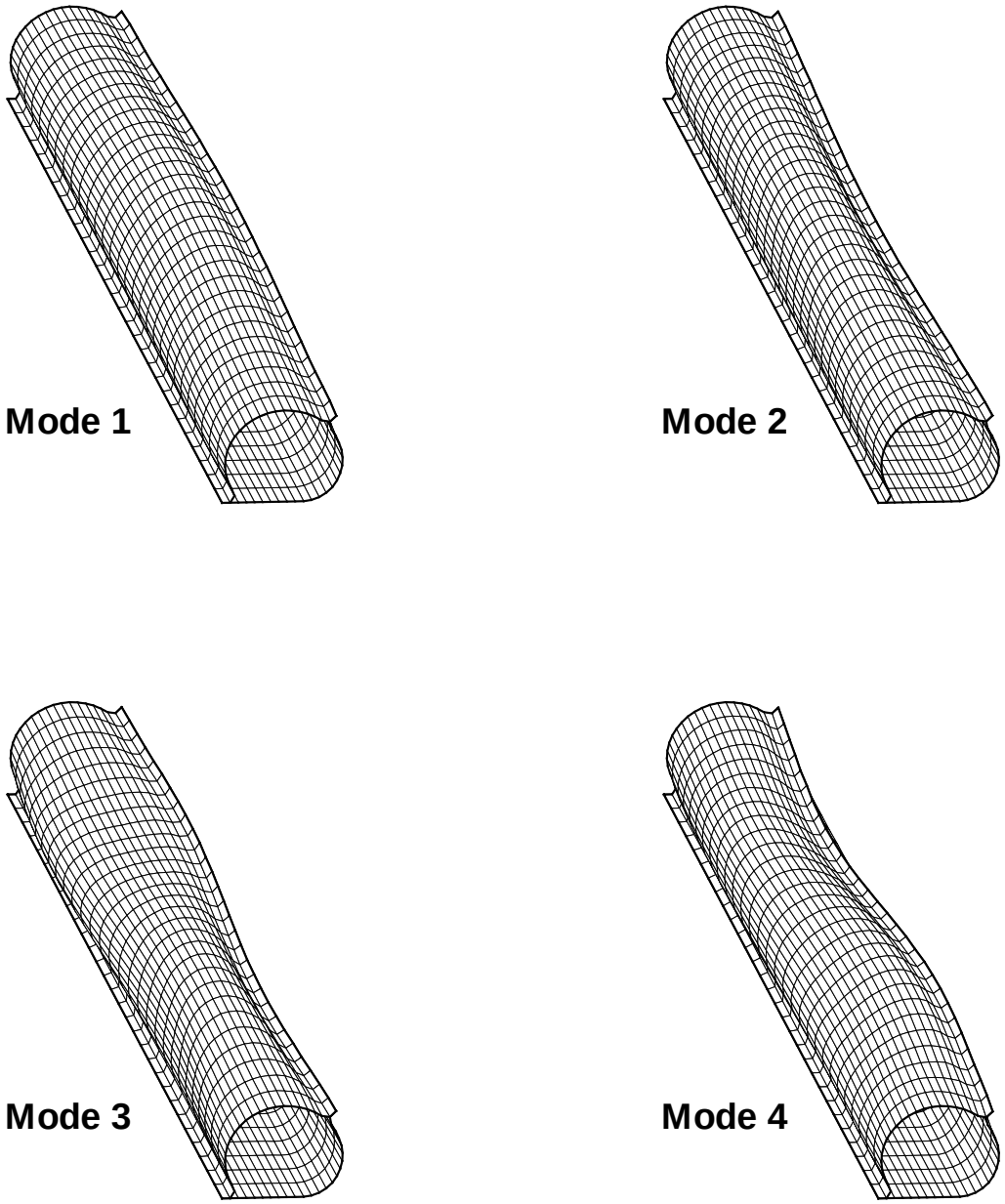

Figure 4.5 First four vibration modes without external water for p_{int} = 1 kPa.

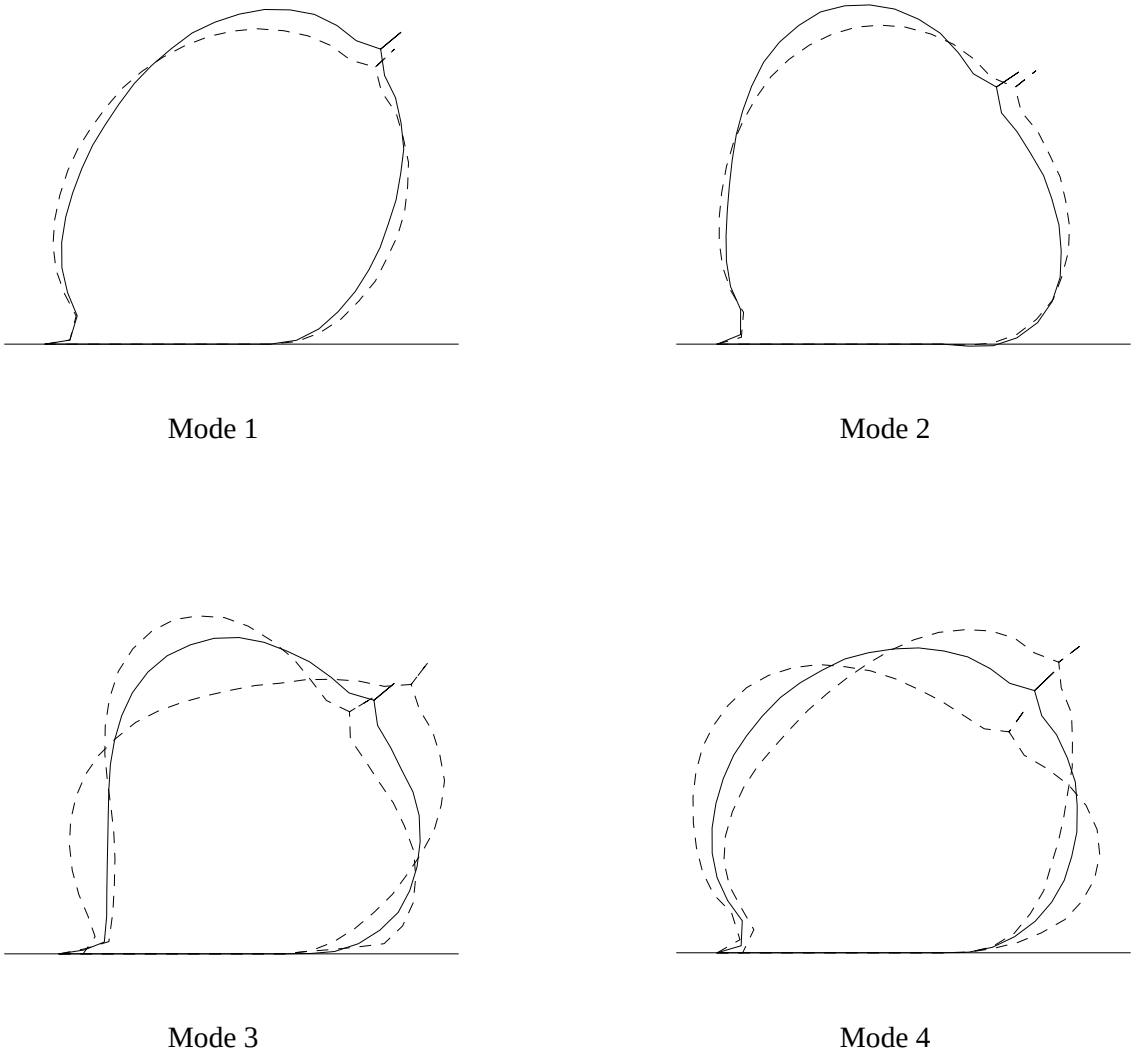

Figure 4.6 Cross-sections of modes in Figure 4.5 at the center (solid curves) and at the quarter lengths from the ends (dashed curves).

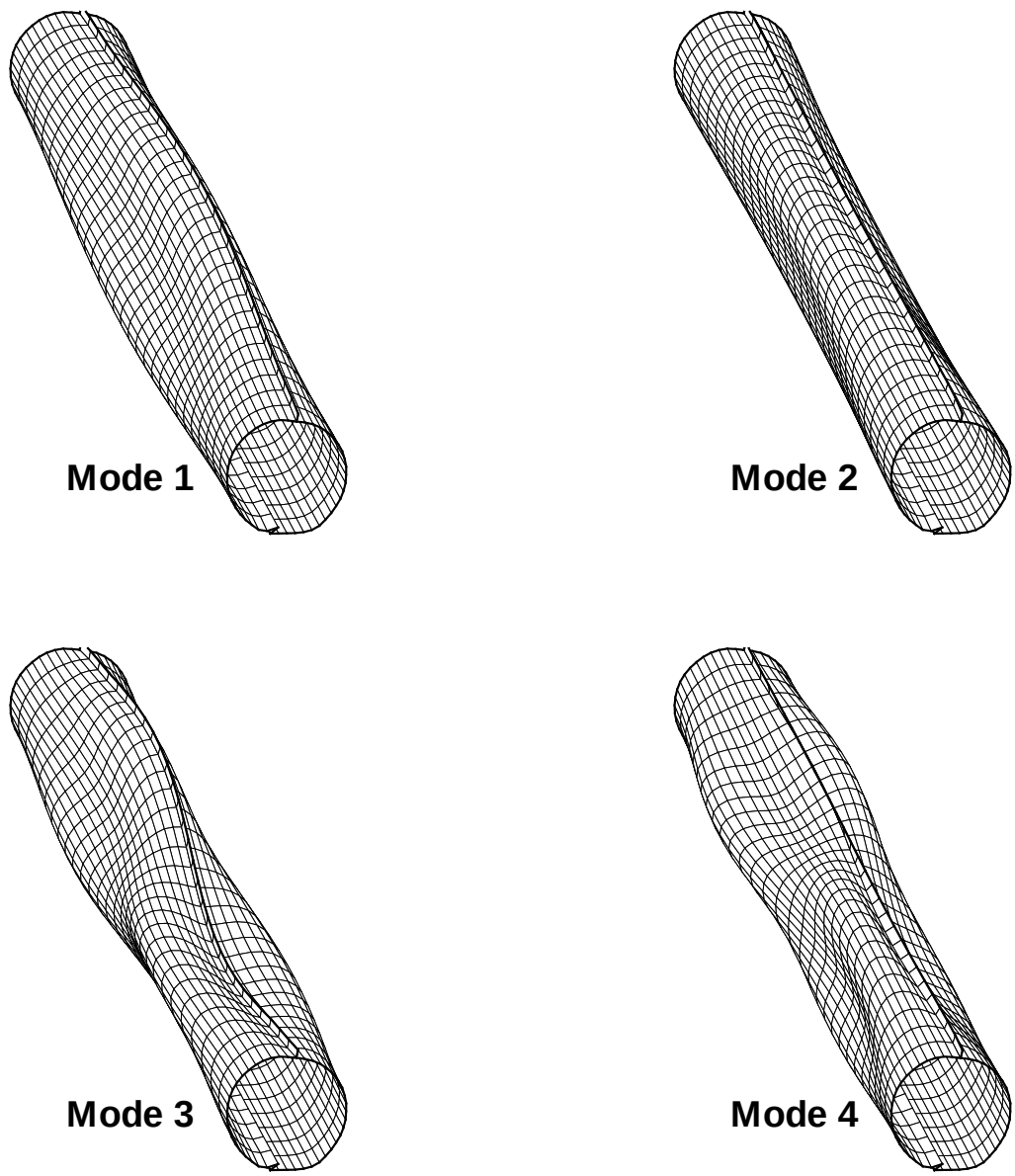

Figure 4.7 First four vibration modes without external water for p_{int} = 30 kPa.

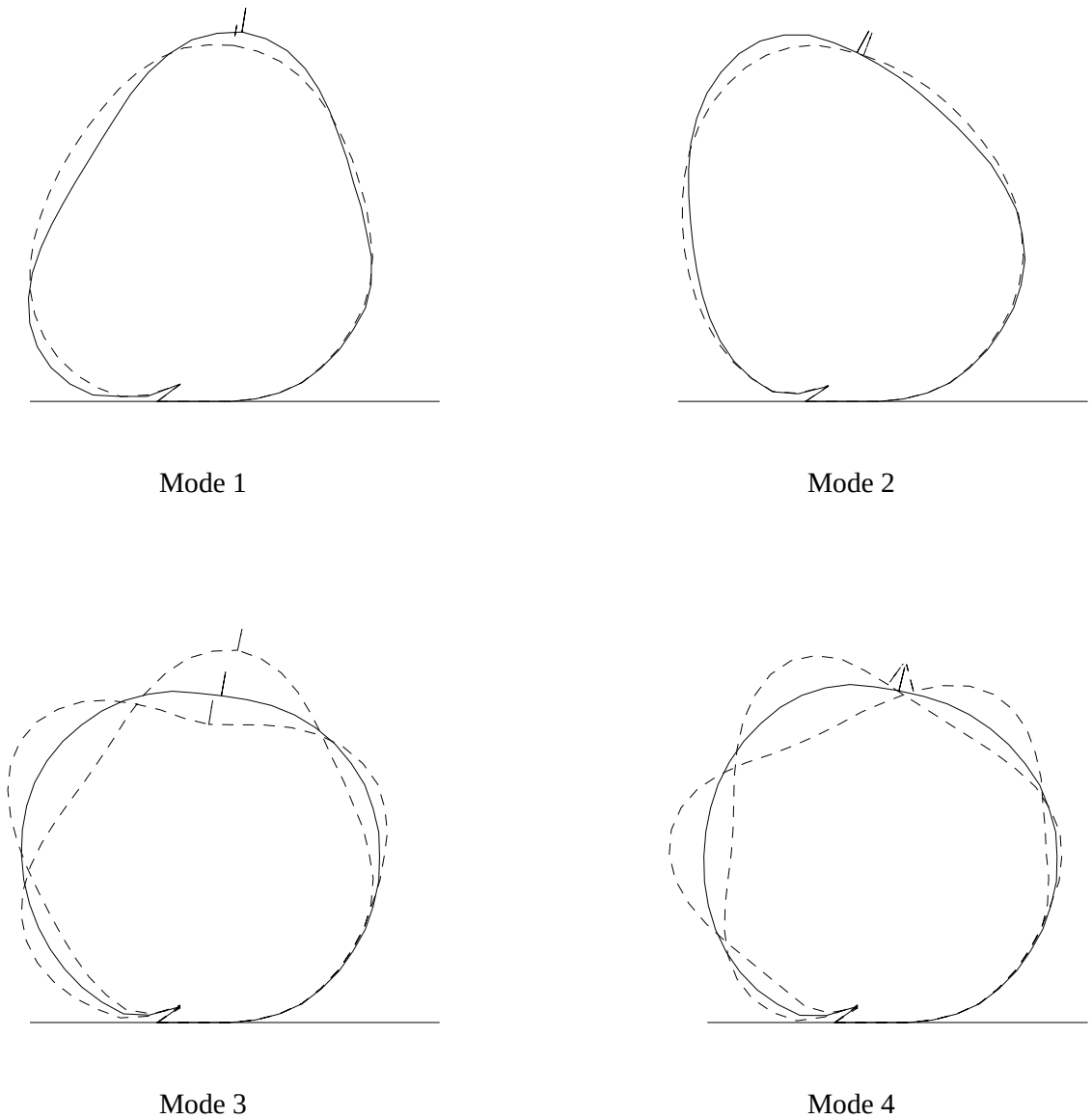

Figure 4.8 Cross-sections of modes in Figure 4.7 at the center (solid curves) and at quarter lengths from the ends (dashed curves).

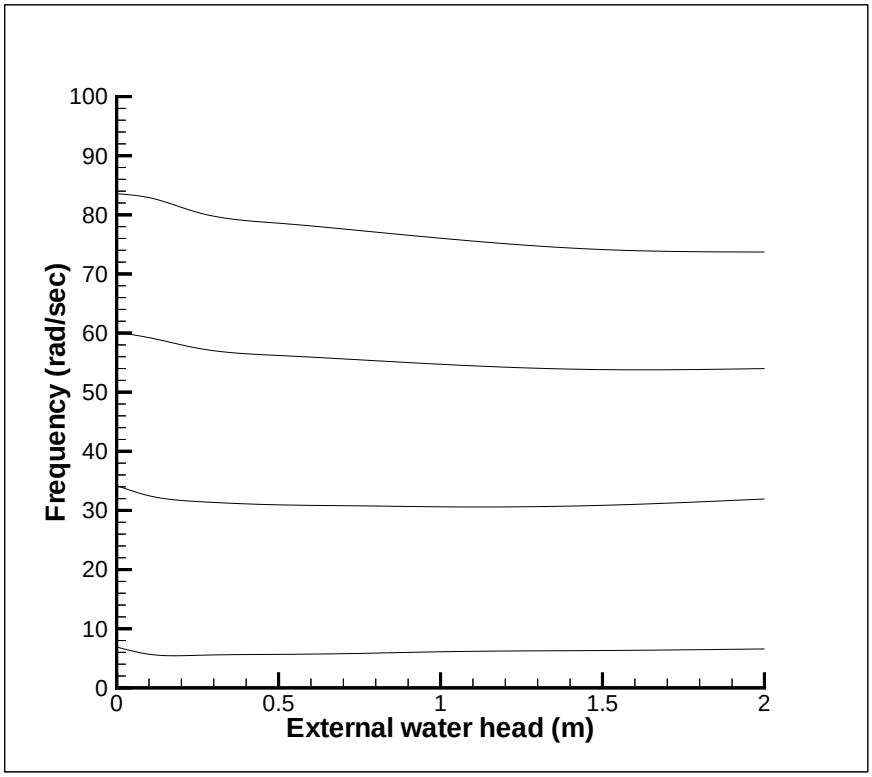

Figure 4.9 Variation of frequency with external water head; (p_{int} = 30 kPa)

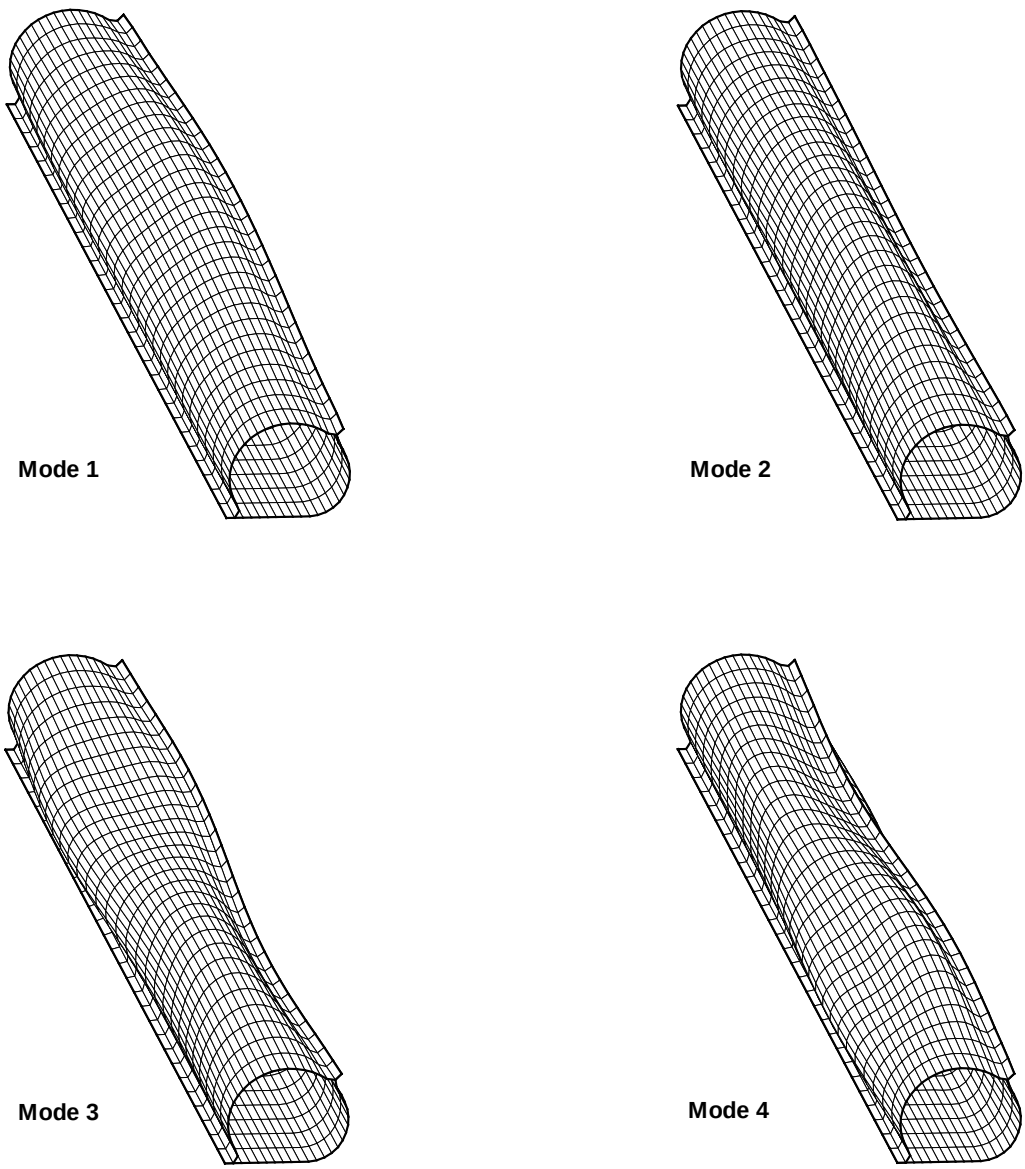

Figure 4.10 First four vibration modes with external water for p_{int} = 1 kPa.

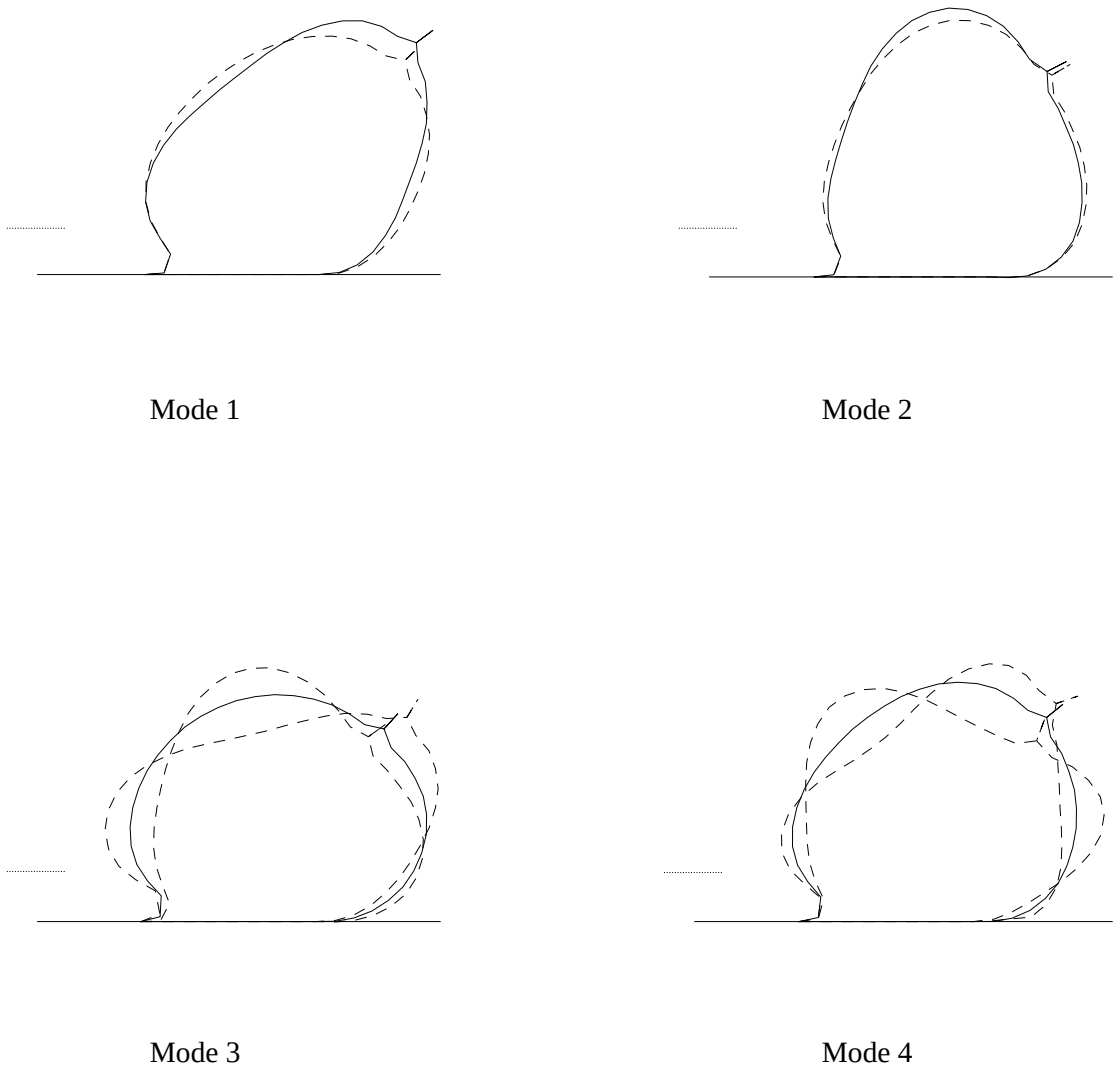

Figure 4.11 Cross-sections of the modes in Figure 4.10 at the center (solid curves) and at quarter-lengths from the ends (dashed curves).

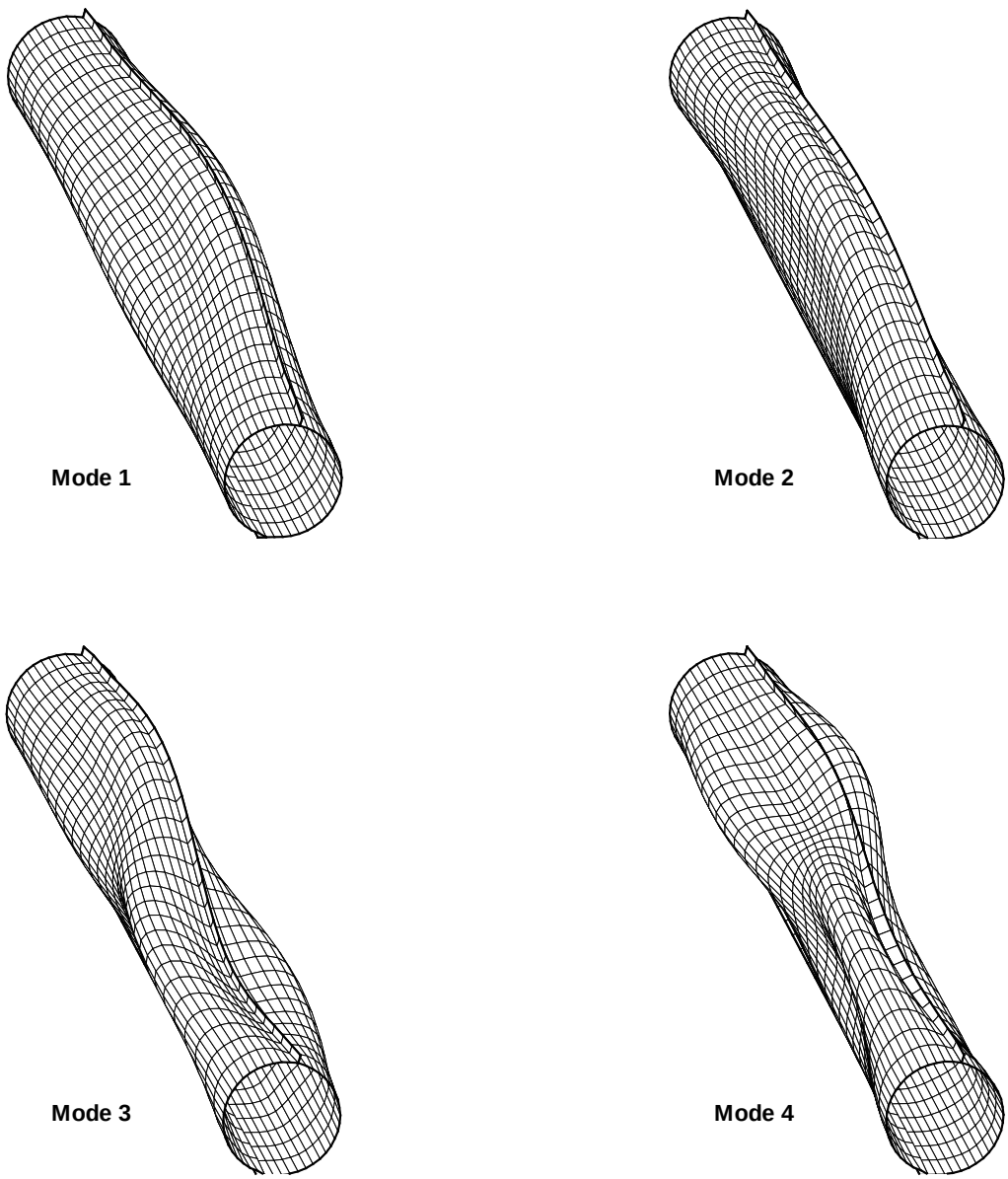

Figure 4.12 First four vibration modes with external water for p_{int} = 30.0 kPa.

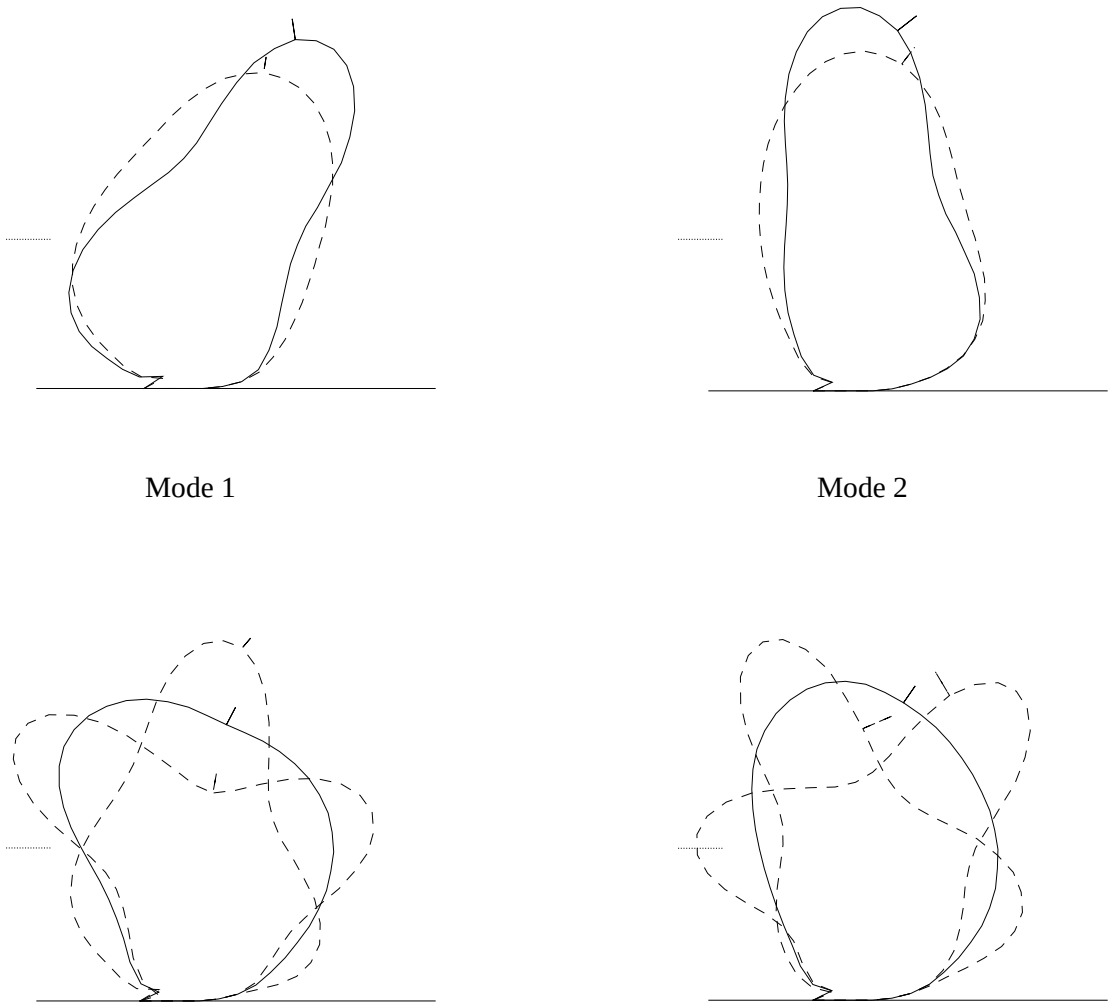

Figure 4.13 Cross-sections of the modes in Figure 4.12 at the center (solid curves) and at quarter-lengths from the ends (dashed curves).

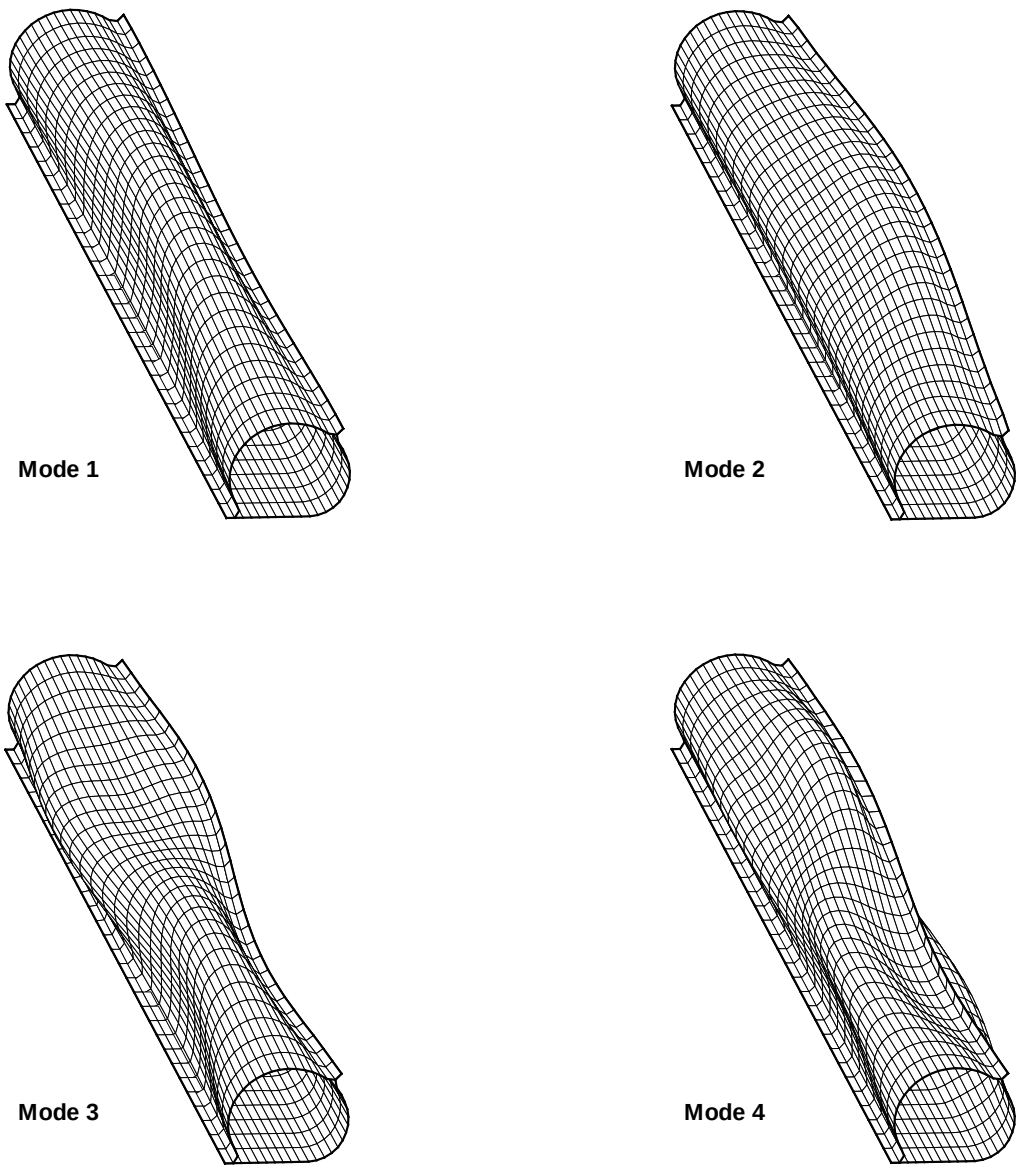

Figure 4.14 First four vibration modes with parallel flow of 1 m/s, for p_{int} = 1 kPa.

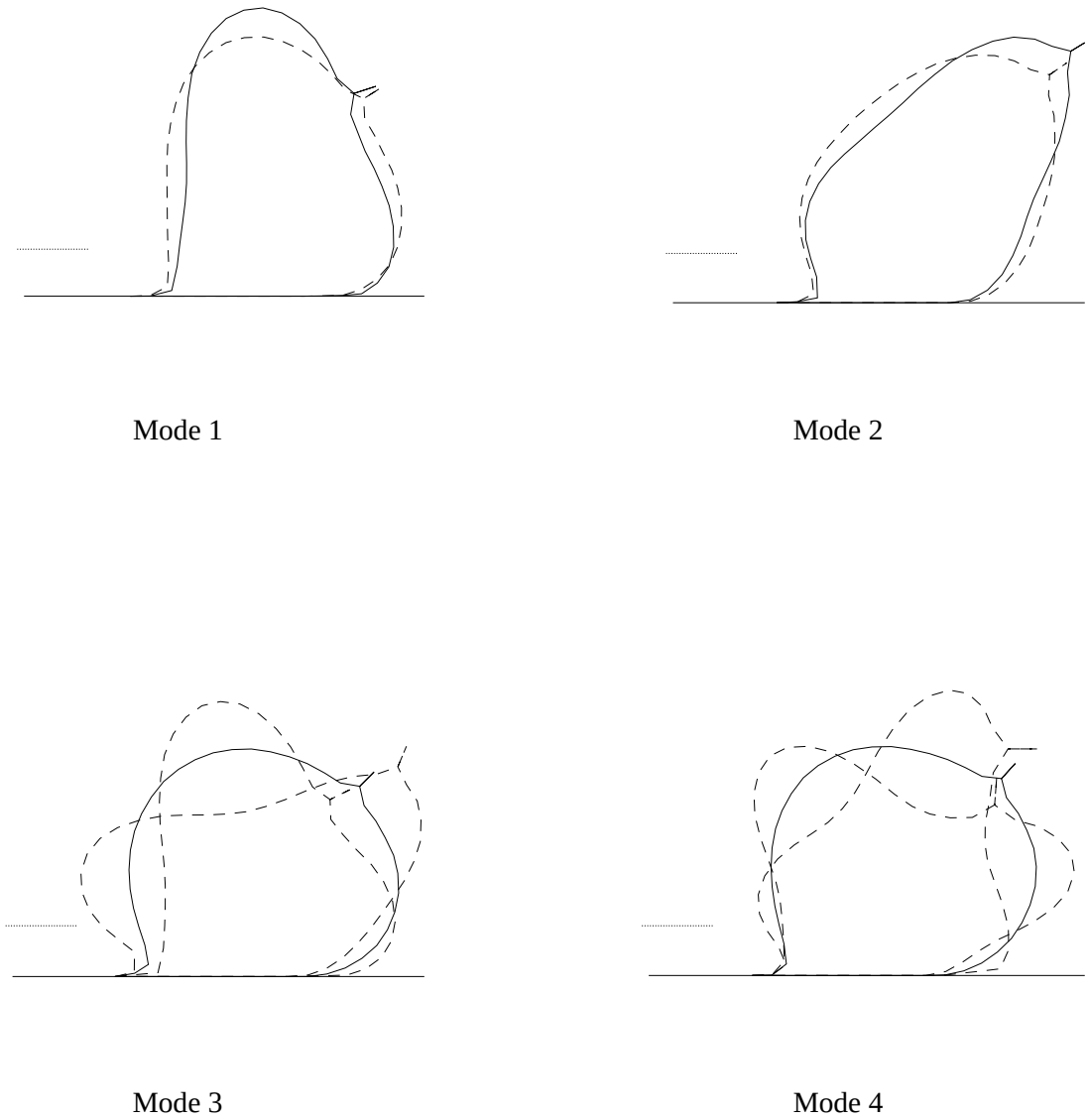

Figure 4.15 Cross-sections of the modes in Figure 4.14 at the center (solid curves) and at quarter-lengths from the ends (dashed curves).

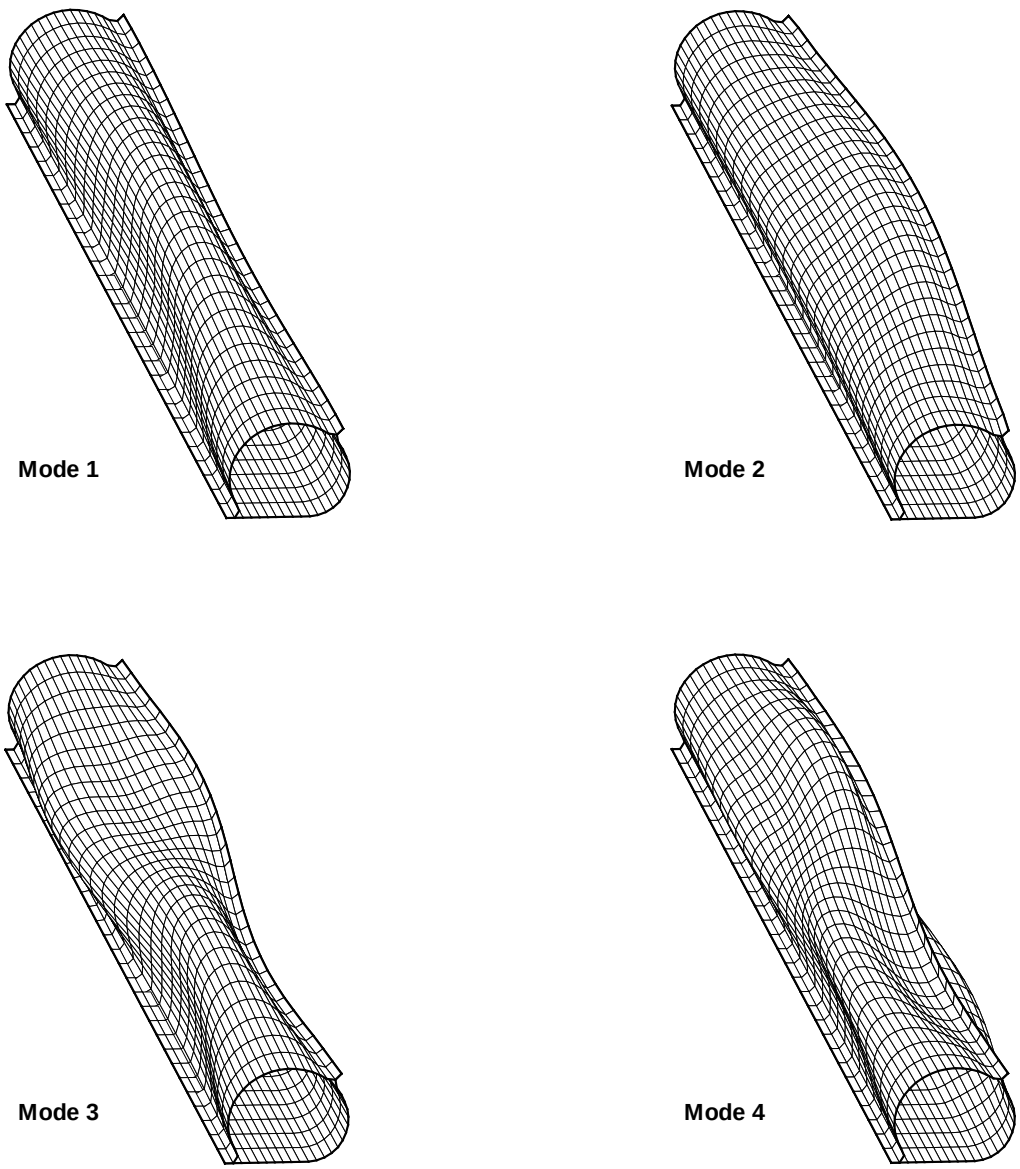

Figure 4.16 First four vibration modes with parallel flow of 5 m/s, for p_{int} = 1 kPa.

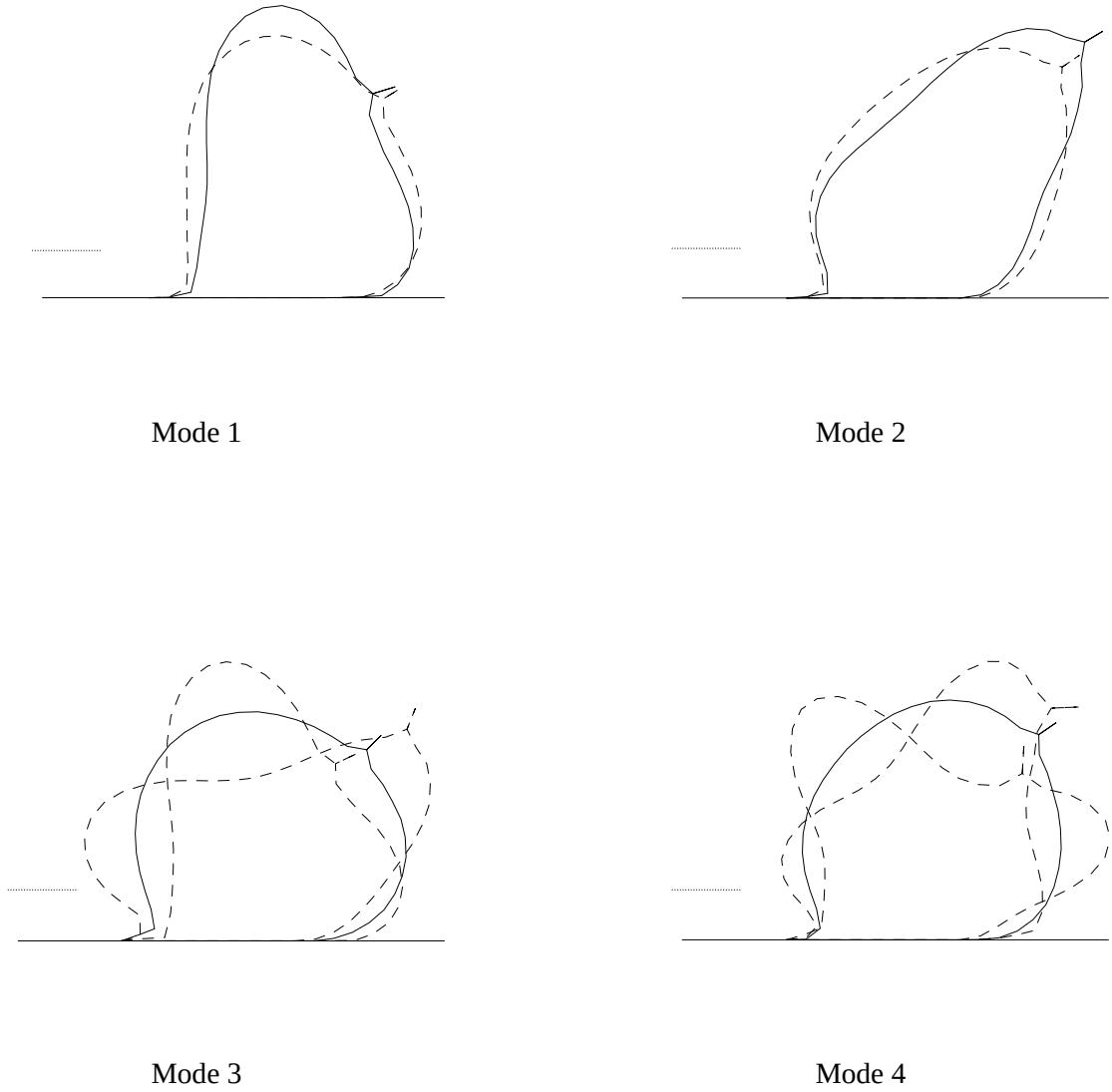

Figure 4.17 Cross-sections of the modes in Figure 4.16 at the center (solid curves) and at quarter-lengths from the ends (dashed curves).

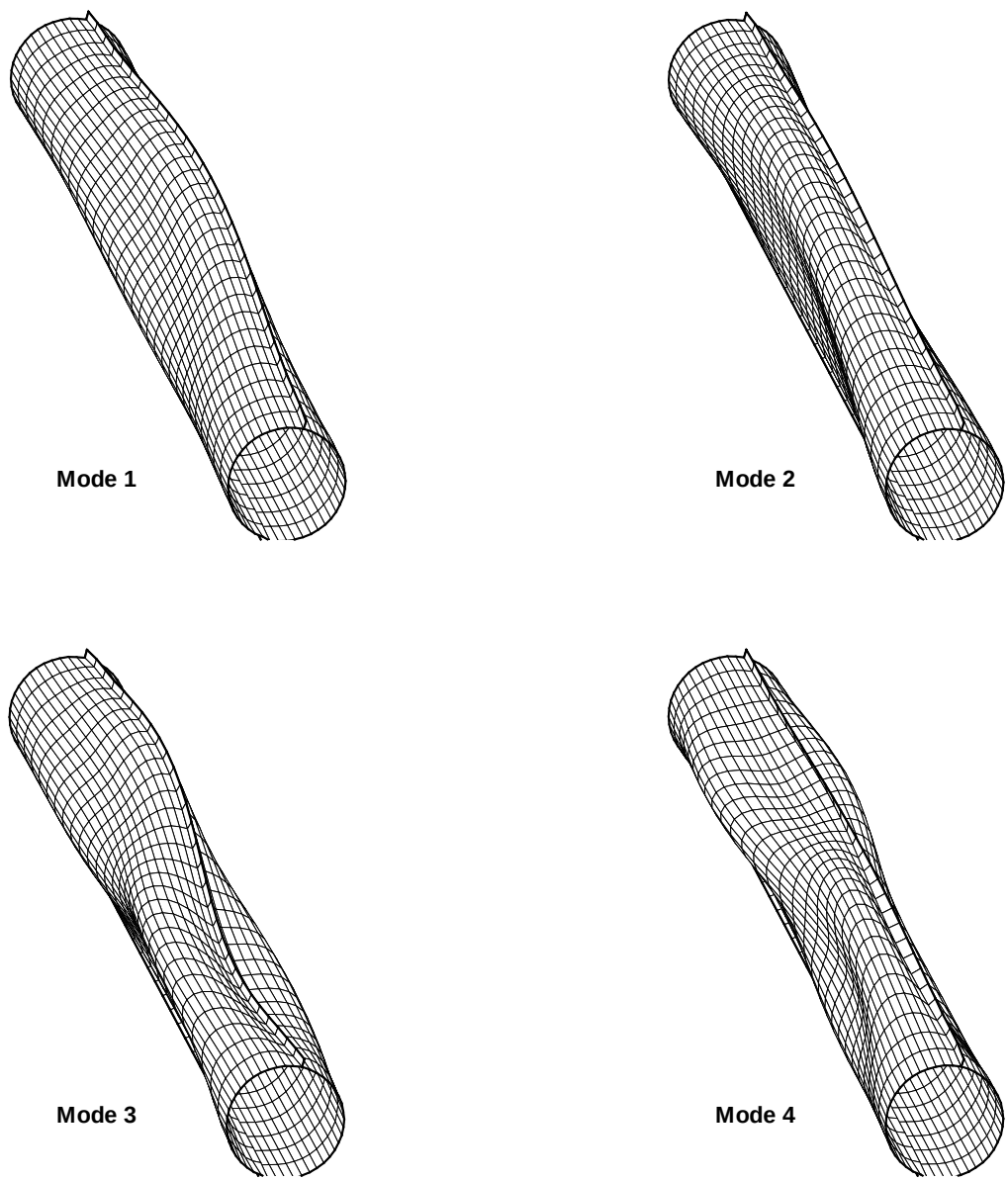

Figure 4.18 First four vibration modes with parallel flow of 1 m/s, for p_{int} = 30 kPa.

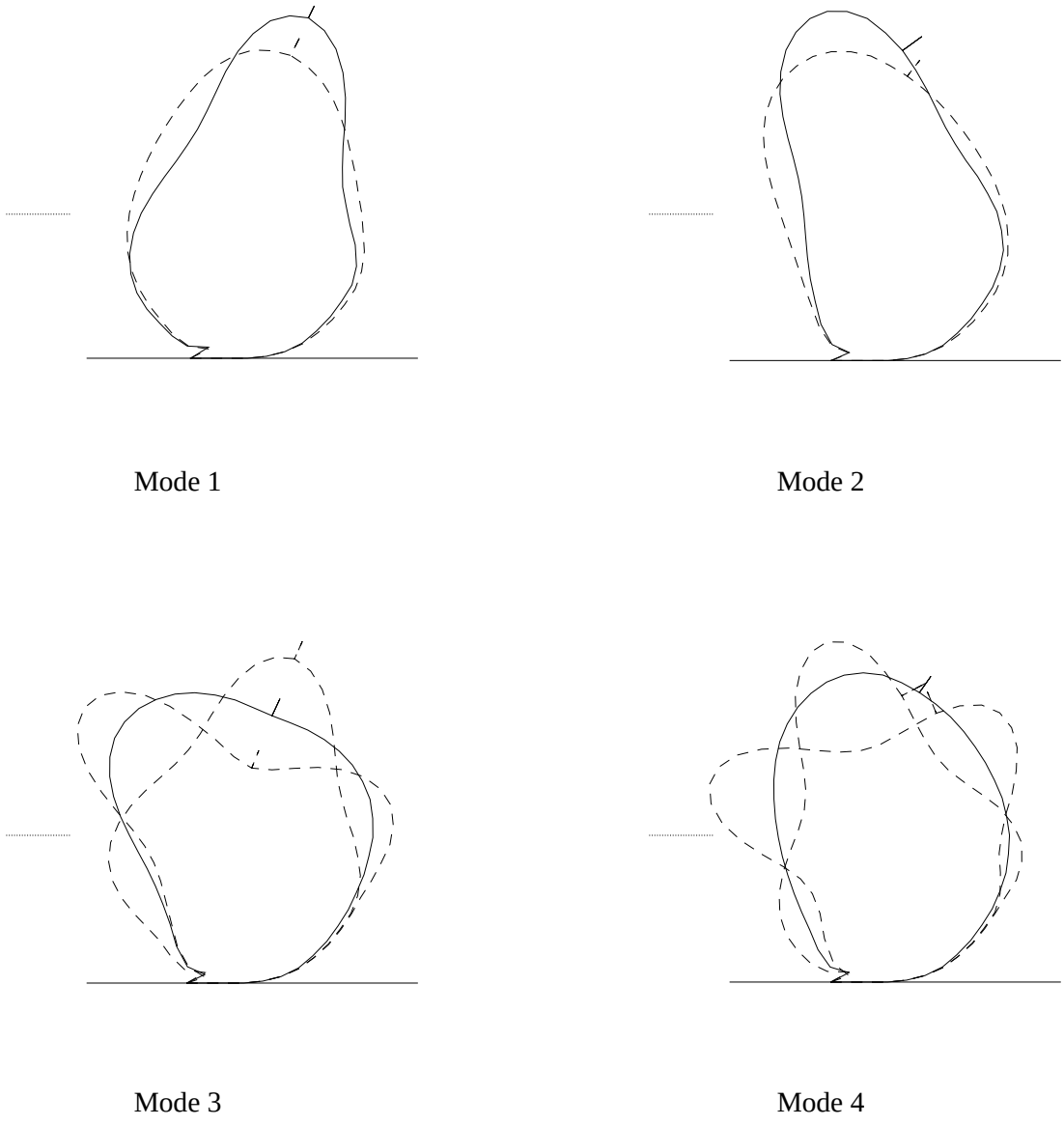

Figure 4.19 Cross-sections of the modes in Figure 4.18 at the center (solid curves) and at quarter-lengths from the ends (dashed curves).

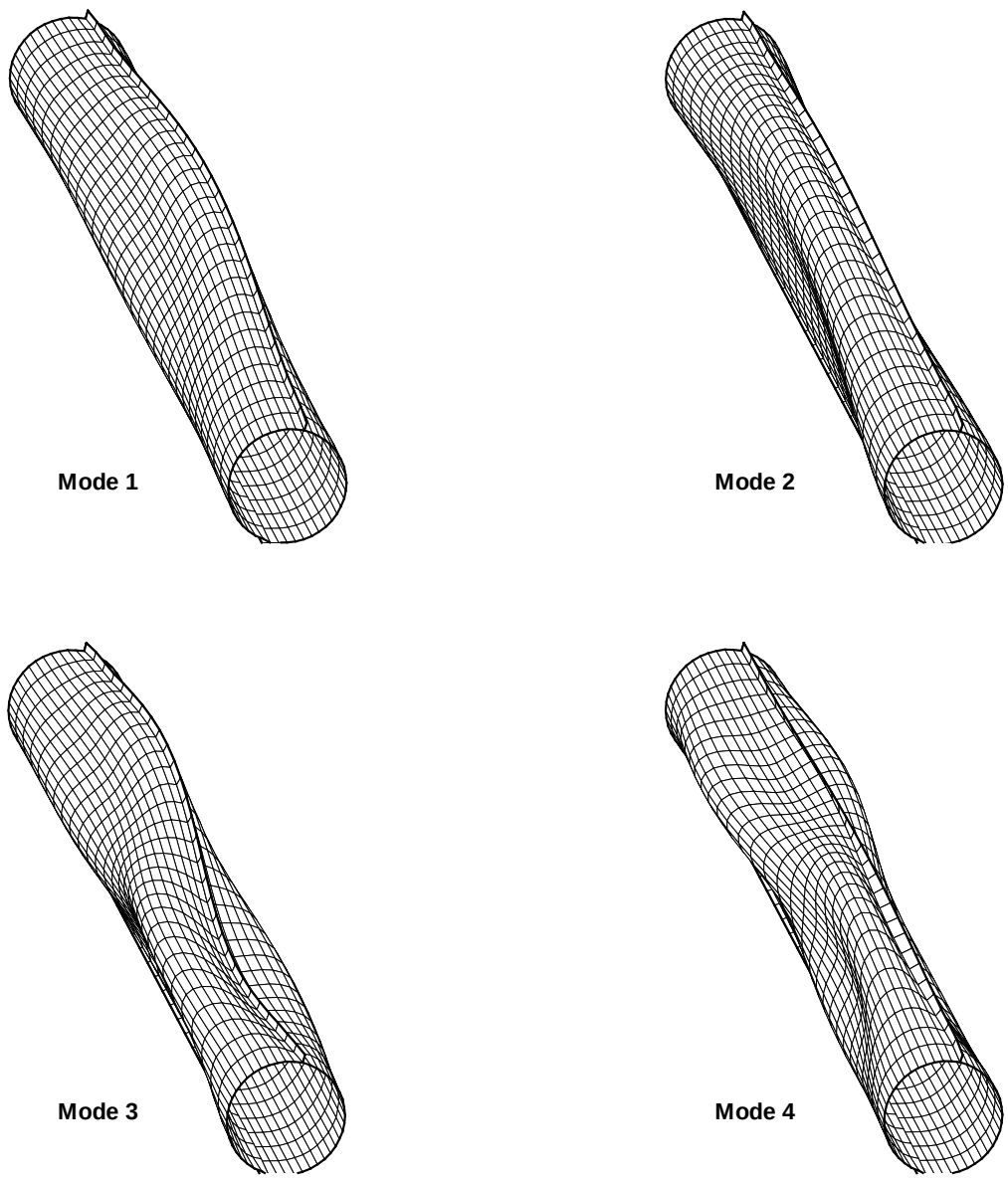

Figure 4.20 First four modes with parallel flow of 5 m/s, for p_{int} = 30 kPa.

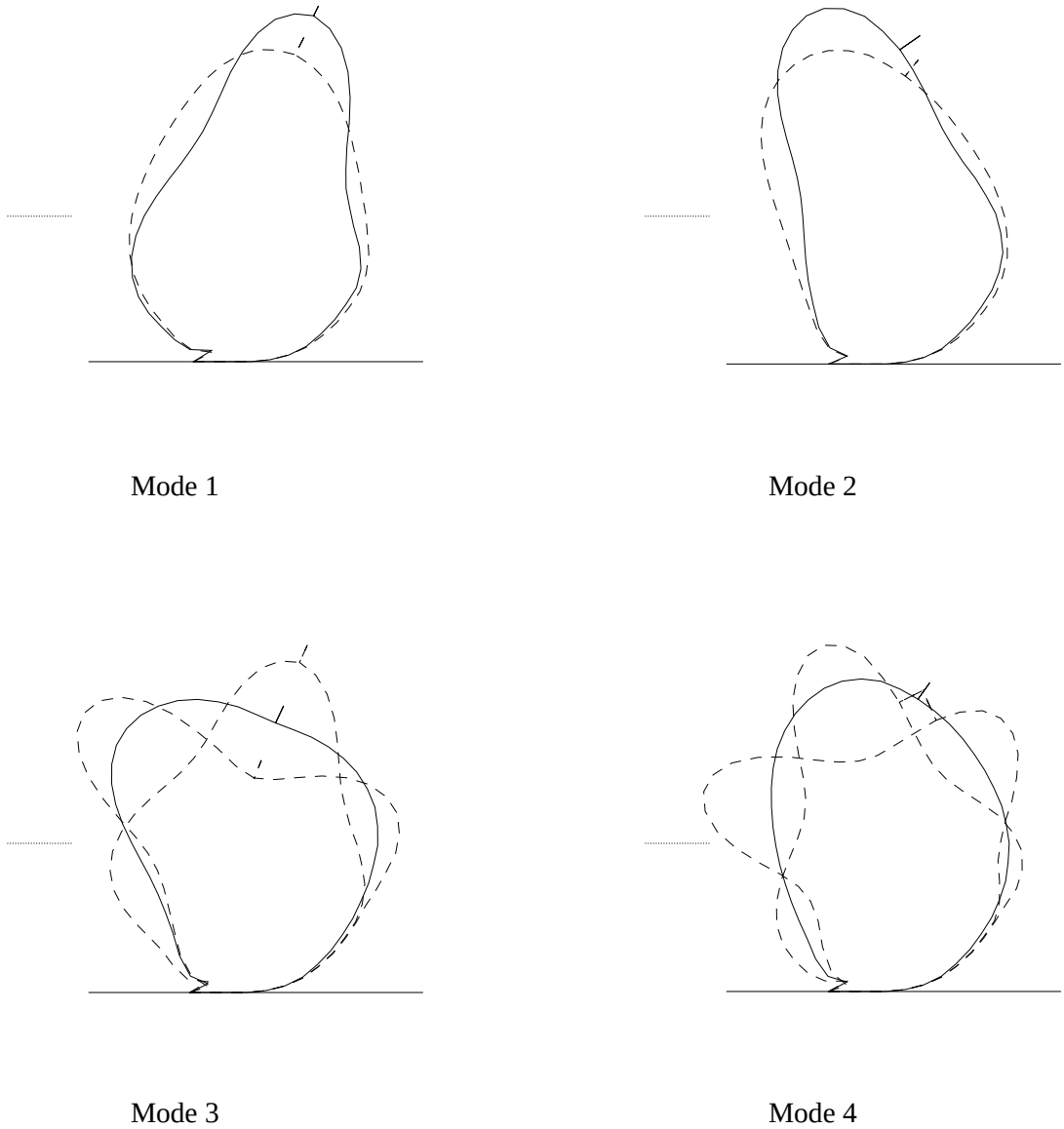

Figure 4.21 Cross-sections of the modes in Figure 4.20 at the center (solid curves) and at quarter-lengths from the ends (dashed curves).

Table 4.1 *Natural frequencies (rad/sec) of a flexible circular cylinder*.

Mode #	Without Water	With Water	Analytical (With Water)
1	**25.53**	**18.49**	**18.05**
2	**51.43**	**37.53**	**36.37**
3	**78.07**	**57.67**	**55.20**
4	**105.9**	**79.54**	**74.89**

Table 4.2 *Natural frequencies (rad/sec) of a double-anchored inflatable dam.*

Mode No.	Without Water		With Water	
	Dakshina Moorthy	Present study	Dakshina Moorthy	Present study
1	**47.3**	**53.55**	**45.6**	**53.51**
2	**55.7**	**61.68**	**55.3**	**59.63**
3	**65.5**	**76.21**	**62.5**	**67.25**
4	**74.2**	**84.23**	**74.8**	**82.45**
5	**82.5**	**92.13**	**77.2**	**91.38**

Table 4.3 *Natural frequencies (rad/sec) of the inflatable dam.*

Mode #	p_{int} = 1 kPa			p_{int} = 30 kPa		
	Without Water	*With Hydrostatic Pressure*	*With Water*	*Without Water*	*With Hydrostatic Pressure*	*With Water*
1	**2.169**	**2.512**	**2.108**	**5.943**	**7.151**	**6.310**
2	**7.775**	**8.785**	**7.401**	**33.32**	**38.58**	**30.87**
3	**13.49**	**14.71**	**12.42**	**60.67**	**67.27**	**53.82**
4	**19.14**	**20.91**	**17.43**	**84.91**	**92.66**	**74.12**

Table 4.4 *Natural frequencies (rad/sec) of the dam with parallel flow, for* p_{int} *= 1 kPa.*

Mode #	Without Water	With Water	U = 1.0 m/s	U = 5.0 m/s
1	**2.169**	**2.108**	**2.011**	**1.995**
2	**7.775**	**7.401**	**7.105**	**6.956**
3	**13.49**	**12.42**	**11.99**	**11.55**
4	**19.14**	**17.43**	**16.47**	**16.03**

Table 4.5 *Natural frequencies (rad/sec) of the dam with parallel flow, for* p_{int} *= 30 kPa.*

Mode #	Without Water	With Water	U = 1.0 m/s	U = 5.0 m/s
1	**5.943**	**6.311**	**6.241**	**6.188**
2	**33.32**	**30.87**	**29.98**	**29.56**
3	**60.67**	**53.82**	**52.61**	**51.98**
4	**84.91**	**74.12**	**72.81**	**70.32**